RESEARCH ARTICLE | NOVEMBER 02 2023

## Tunable bandgap and Si-doping in N-polar AlGaN on C-face 4H-SiC via molecular beam epitaxy

Shubham Mondal ⑩ ; Ding Wang ⑩ ; A F M Anhar Uddin Bhuiyan ⑩ ; Mingtao Hu ⑩ ; Maddaka Reddeppa ⑩ ; Ping Wang ⑩ ; Hongping Zhao ⑩ ; Zetian Mi ➡ ⑩

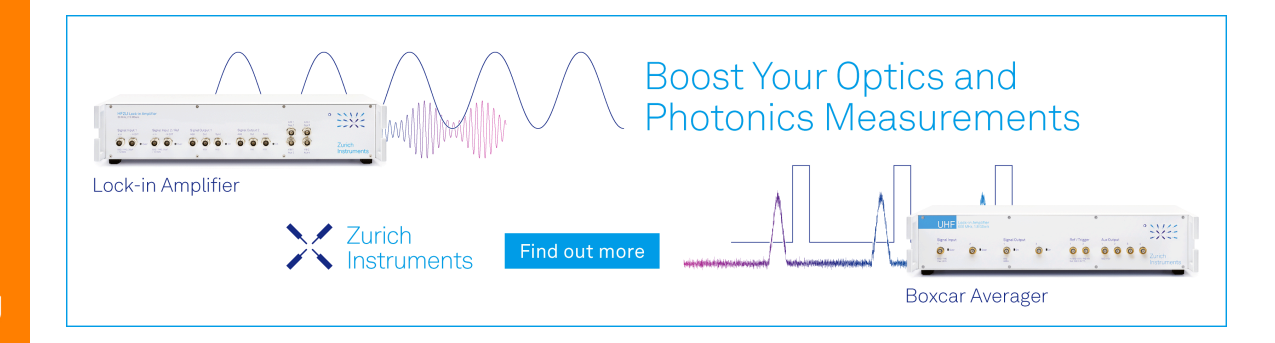


Appl. Phys. Lett. 123, 182106 (2023) https://doi.org/10.1063/5.0173637





CrossMark





# Tunable bandgap and Si-doping in N-polar AlGaN on C-face 4H-SiC via molecular beam epitaxy

Cite as: Appl. Phys. Lett. **123**, 182106 (2023); doi: 10.1063/5.0173637 Submitted: 23 August 2023 · Accepted: 10 October 2023 · Published Online: 2 November 2023







Shubham Mondal, boling Wang, back A F M Anhar Uddin Bhuiyan, bolingtao Hu, boling Maddaka Reddeppa, boling Wang, boling Wang, boling Wang, boling Wang, boling Zhao, boling A F M Anhar Uddin Bhuiyan, boling Mingtao Hu, boling Maddaka Reddeppa, boling Wang, boling Maddaka Reddeppa, boling Wang, boling Wan

### **AFFILIATIONS**

- <sup>1</sup>Department of Electrical Engineering and Computer Science, University of Michigan, Ann Arbor, Michigan 48109, USA
- $^2$ Department of Electrical and Computer Engineering, The Ohio State University, Columbus, Ohio 43210, USA

### **ABSTRACT**

N-polar AlGaN is an emerging wide-bandgap semiconductor for next-generation high electron mobility transistors and ultraviolet light emitting diodes and lasers. Here, we demonstrate the growth and characterization of high-quality N-polar AlGaN films on C-face 4H-silicon carbide (SiC) substrates by molecular beam epitaxy. On optimization of the growth conditions, N-polar AlGaN films exhibit a crack free, atomically smooth surface (rms roughness  $\sim 0.9$  nm), and high crystal quality with low density of defects and dislocations. The N-polar crystallographic orientation of the epitaxially grown AlGaN film is unambiguously confirmed by wet chemical etching. We demonstrate precise compositional tunability of the N-polar AlGaN films over a wide range of Al content and a high internal quantum efficiency  $\sim$ 74% for the 65% Al content AlGaN film at room temperature. Furthermore, controllable silicon (Si) doping in high Al content (65%) N-polar AlGaN films has been demonstrated with the highest mobility value  $\sim$ 65 cm²/V-s observed corresponding to an electron concentration of  $1.1 \times 10^{17}$  cm<sup>-3</sup>, whereas a relatively high mobility value of 1.8 cm²/V-s is sustained for an electron concentration of  $3.2 \times 10^{19}$  cm<sup>-3</sup>, with an exceptionally low resistivity value of 0.009  $\Omega$ -cm. The polarity-controlled epitaxy of AlGaN on SiC presents a viable approach for achieving high-quality N-polar III-nitride semiconductors that can be harnessed for a wide range of emerging electronic and optoelectronic device applications.

Published under an exclusive license by AIP Publishing. https://doi.org/10.1063/5.0173637

In recent years, III-nitrides have deeply penetrated the realms of photonic and electronic devices, catalyzing disruptive technological advancements in high-power and high-frequency electronics, optoelectronics, and clean energy. 1-5 Within this expansive domain of applications, two notable areas have garnered significant interest. First, the utilization of III-nitride semiconductors in deep ultraviolet (UV) optoelectronics, including light-emitting diodes (LEDs) and lasers, has emerged as a compelling solution for sterilization and water/air purification.<sup>6-8</sup> Second, there has been significant progress in developing next-generation ultra-wide-bandgap high-electron mobility transistors (HEMTs) that possess high breakdown fields and efficient thermal management.<sup>2,9–11</sup> The successful implementation of these promising technologies relies on the utilization of tunable aluminum content AlGaN layers with a precise control over doping levels spanning multiple orders of magnitude. The upper range of doping enables the realization of high electrical conductivity in injection layers for deep UV LEDs and lasers, whereas the lower range facilitates the creation of low-doped drift regions in HEMTs.<sup>7,12</sup> While the majority of studies have been focused on metal-polar III-nitride semiconductors, there has been a recent surge in interest regarding the distinct advantages offered by their nitrogen (N) polar counterparts. 13,14 In the realm of HEMTs, the N-polar GaN/AlGaN heterostructure naturally forms a back barrier, contributing to enhanced carrier confinement, reduced contact resistance, and improved gate control compared to metalpolar devices. 15,16 On the other hand, for optoelectronic devices like LEDs and laser diodes, the N-polar configuration offers notable advantages, such as reduced electron overflow and enhanced electrical efficiency, surpassing the performance of their metal-polar counterparts. 14,17 To date, however, the realization of high-quality Npolar Al(Ga)N has remained extremely challenging. <sup>18</sup> Previous reports of N-polar Al(Ga)N grown on substrates, such as sapphire and silicon, are plagued with the presence of high densities of dislocations, due to the large lattice mismatch and the formation of inversion domains and poor surface morphology. 18-21 In contrast, the direct epitaxy of

<sup>&</sup>lt;sup>3</sup>Department of Materials Science and Engineering, The Ohio State University, Columbus, Ohio 43210, USA

a) Author to whom correspondence should be addressed: ztmi@umich.edu

N-polar Al(Ga)N on an AlN bulk substrate encounters severe limitations primarily due to the prohibitively high cost associated with the substrate, making this approach unscalable. <sup>22,23</sup>

Prior investigations utilizing MOCVD techniques have demonstrated the successful attainment of N-polar III-nitrides on 4H-silicon carbide (SiC) substrates with a C-face orientation.<sup>24–26</sup> SiC is especially promising in this application space owing to its excellent thermal conductivity, wide bandgap, low cost, and, importantly, minimal lattice mismatch ( $\sim$ 1%) between AlN (3.112 Å) and 4H-SiC (3.08 Å), which allows for the seamless epitaxial growth of high-quality III-nitride layers with minimal defects and dislocations. 27,2 In contrast to MOCVD, molecular beam epitaxy (MBE) growth presents significant advantages, including significantly reduced impurity incorporation, precise control over doping, and the flexibility to tune the composition especially in Al-rich AlGaN. <sup>28–30</sup> Previous reports have demonstrated the epitaxy of metal-polar AlGaN on Si-face of 4H-SiC substrates by MBE and MOCVD. However, growth of N-polar III-nitride is more involved than its metal-polar counterpart, primarily due to the small adatom diffusion length owing to a high binding energy on the Npolar surface.<sup>24</sup> This promotes the formation of islands and other surface irregularities. <sup>26,3</sup>, As such, there have been no reports on the epitaxy of N-polar AlGaN on C-face SiC by MBE.

In this study, we present a detailed experimental investigation of the epitaxy and structural, optical, and electrical properties of N-polar AlGaN on C-face 4H-SiC substrates with compositions varying across the entire alloy range. The epitaxially grown N-polar surface is atomically smooth and free of pits or cracks. The N-polar orientation of the epitaxial AlGaN layers has been confirmed by wet chemical etching. The strain-state analysis by XRD reciprocal-space mapping reveals an in-plane compressive stress in the epitaxially grown AlGaN films, which reduces with increasing Al content. The Al content in AlGaN has been systematically varied from 0% (GaN) to 20%, 40%, 65%, and 100% (AlN) to enable a precise control over the bandgap, leading to tunable photoluminescence (PL) characteristics. Temperaturedependent PL measurements conducted on the AlGaN alloy with a high aluminum (Al) content of 65% demonstrate a high internal quantum efficiency (IQE) of 74% at room temperature. Precise control over Si doping spanning multiple orders of magnitude has been achieved in high aluminum (Al) content (65%) AlGaN films. The measured Hall mobility reaches up to 65 cm<sup>2</sup>/V-s at an electron concentration of  $1.1 \times 10^{17} \, \text{cm}^{-3}$ , and a relatively high mobility value of  $18 \, \text{cm}^2/\text{V-s}$  is sustained for an electron concentration of 3.2 × 10<sup>19</sup> cm<sup>-3</sup>, accompanied by an exceptionally low resistivity of 0.009  $\Omega$ ·cm.

Prior to loading in the MBE chamber, the samples were cleaned via a standard solvent cleaning process. The substrates were then baked and outgassed at 200 and 600 °C in the MBE load-lock and preparation chamber, respectively. Prior research has underscored the significance of surface cleaning before MBE growth of AlN for preventing polarity inversion on the oxidized regions. The samples were then annealed for 10 min inside the growth chamber at a thermocouple temperature of 1000 °C to further promote the desorption of surface oxides, resulting in the generation of a pristine growth front. A Veeco GENxplor MBE system equipped with a radio frequency (RF) nitrogen (purity 99.9999%) plasma source and Knudsen effusion cells for Ga (purity 99.999 99%) and Al (purity 99.999 95%) was utilized to epitaxially grow 200 nm AlN buffer, followed by 200 nm AlGaN films on the C-face of 4H-SiC substrates with a miscut of 4°, schematically shown in Fig. 1(a).

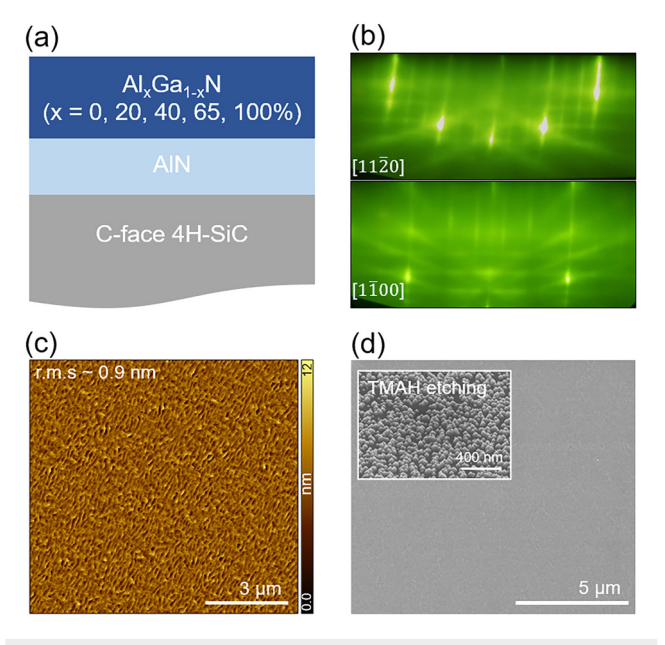


**FIG. 1.** (a) Schematic illustration of the AlGaN/AlN/SiC heterostructure. (b) RHEED patterns recorded at the end of AlGaN layer growth showing clear reconstruction lines indicative of a smooth surface morphology. (c) AFM image of the AlGaN surface showing atomically smooth surface with an rms roughness of 0.9 nm for a  $10 \times 10~\mu\text{m}^2$  scanning area. (d) SEM image showing featureless AlGaN surface. Inset: post-TMAH etching SEM image confirms the N-polar crystallographic orientation of the epitaxially grown AlGaN.

Due to the relatively small lattice mismatch of  $\sim$ 1% between AlN and SiC, AlN serves as a favorable template for the epitaxial growth of AlGaN. Furthermore, this layer serves to inhibit the incorporation of undesirable impurities, such as Si, O, and C, in the subsequently grown AlGaN epilayers. Reflection high energy electron diffraction (RHEED) was utilized to monitor the entire growth. Figure 1(b) illustrates the observed RHEED patterns of the AlGaN epilayer along two different azimuths. The presence of bright, streaky lines accompanied by a  $2 \times 2$ reconstruction signifies the attainment of an atomically smooth surface. To further characterize the AlGaN epilayers, atomic force microscopy (AFM) measurements were conducted, revealing a root mean square (rms) roughness of 0.9 nm across a scanning area of  $10 \times 10 \,\mu\text{m}^2$  for the 65% Al content AlGaN sample, as depicted in Fig. 1(c). The growth of N-polar III-nitrides is characterized by adatoms exhibiting a restricted diffusion length on N-polar surfaces, which can be attributed to their high binding energy. This phenomenon often gives rise to island formation, leading to a rough surface that renders device fabrication infeasible. In our growth studies, we systematically optimized the III/N ratio and growth temperature to identify an optimum growth window that facilitates the achievement of an atomically smooth surface without formation of islands.

Owing to the presence of a  $4^{\circ}$  miscut in the SiC substrates, the surface morphology is prone to step bunching, often resulting in a high surface roughness (rms > 3 nm) as has been observed in previous reports of epitaxy of AlN on similar miscut SiC substrates. <sup>24</sup> In this context, the measured surface roughness of 0.9 nm for a large scanning area  $(10 \times 10 \, \mu \text{m}^2)$  in our N-polar AlGaN films, depicted in Fig. 1(c), is exceptionally low. Figure 1(d) shows an SEM image of the N-polar

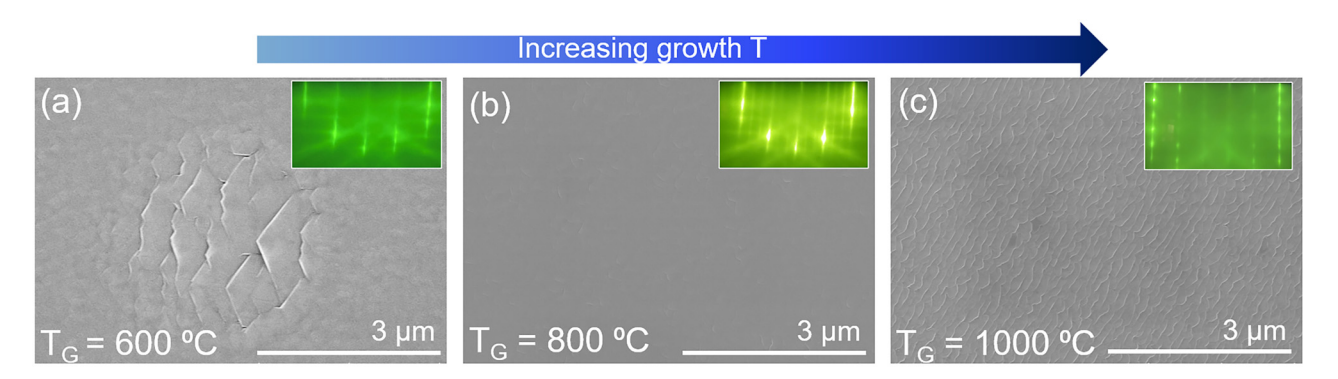


FIG. 2. SEM image of the N-polar AlGaN surface at different growth temperatures along with RHEED patterns (insets). (a) Low growth temperature leads to the formation of pits. (b) Smooth surface morphology at a relatively high growth temperature. (c) Too high growth temperature leads to a rough surface.

AlGaN surface, further confirming the absence of any significant pits or features on the surface. The N-polar crystallographic orientation of the epitaxially grown AlGaN film is unambiguously confirmed by wet chemical etching, as shown in the inset in Fig. 1(d). The sample for Figs. 1(b)–1(d) has been grown at the optimized temperature  $\sim\!800\,^{\circ}\mathrm{C}$  along with a III/V ratio of 3:1, which will be discussed later.

As shown in the SEM images of the 65% Al content AlGaN sample in Figs. 2(a) and 2(c), the surface morphology evolves drastically with variations in growth temperature. A relatively low growth temperature, in the same range used for metal polar AlGaN growth by MBE, leads to the formation of pits, as seen in Fig. 2(a). Owing to the low adatom mobility on the N-polar surface, the metal atoms coalesce in some regions that leads to localized low growth rates in these regions compared to the bulk. On the other hand, a very high growth temperature, although avoiding the formation of pits, leads to a rough surface morphology due to high desorption of Al atoms. This is also reflected in the RHEED patterns observed during the AlGaN growth as shown in the insets in Fig. 2. Thus, to obtain an atomically smooth surface morphology, an optimum growth temperature ~800°C is used along with a III/V ratio of 3:1, wherein the adatom mobility is

enhanced owing to the high temperature, but the desorption of the metal atoms is relatively low. This is underscored by the presence of bright and streaky RHEED patterns, depicted in Fig. 2(b) and the inset, along with the emergence of reconstruction lines.

In order to comprehensively examine the strain state of the AlGaN films grown on AlN/SiC, we measured the reciprocal-space maps (RSMs) derived from the x-ray diffraction patterns performed using a Bruker D8 Discover with Cu Ka radiation x-ray source  $(\lambda = 1.5418 \text{ Å})$ . Figures 3(a)-3(c) display the RSM spectra acquired around the SiC (108)/AlN (104) peaks for three separate samples: (i) AlN, (ii) Al<sub>0.4</sub>Ga<sub>0.6</sub>N/AlN, and (iii) Al<sub>0.65</sub>Ga<sub>0.35</sub>N/AlN epitaxially grown on C-face 4H-SiC. The vertical and tilted dashed lines represent fully strained and fully relaxed positions of the AlGaN films grown on AlN layer, respectively. The presence of a well-defined center in the mosaic spread of both the AlN and AlGaN spots suggests that the growth of the AlN and AlGaN epilayers was characterized by a high degree of crystalline alignment and structural coherence. It can be observed that with increasing Al content from 40% to 65%, the out-ofplane reciprocal-space lattice constant Qz moves closer to the AlN peak. Moreover, with an increase in Al content, it is observed that the

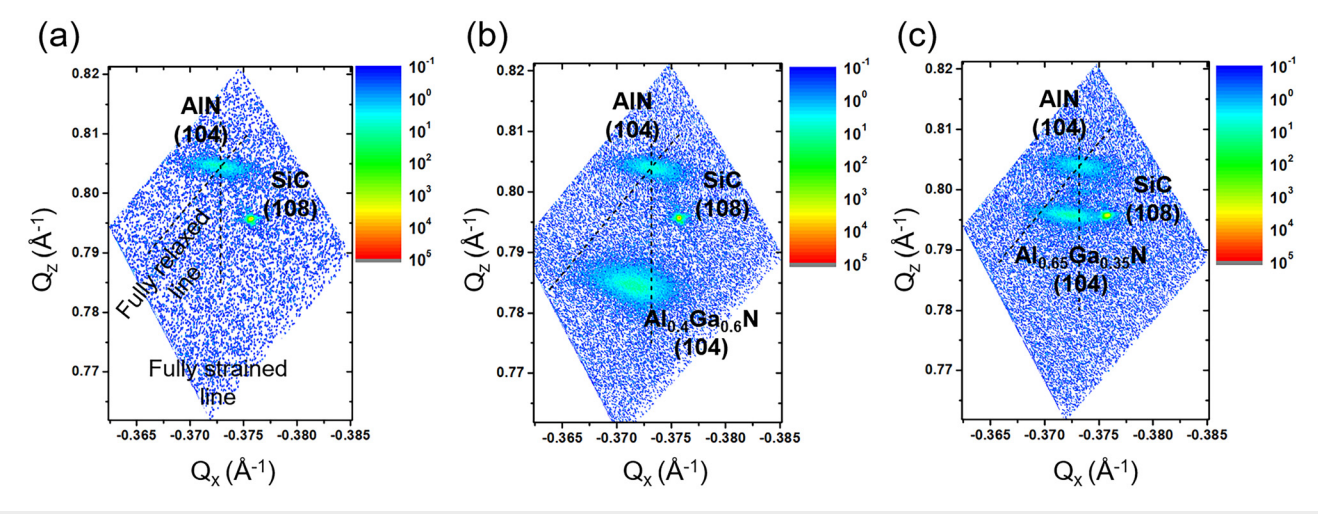


FIG. 3. XRD asymmetrical reciprocal-space maps (RSMs) for (a) AlN/SiC, (b) Al<sub>0.4</sub>Ga<sub>0.6</sub>N/SiC, and (c) Al<sub>0.65</sub>Ga<sub>0.35</sub>N/SiC showing the fully relaxed and fully strained lines and the corresponding position of the maximum reflection intensity of AlGaN reciprocal lattice points.

maximum reflection intensity of AlGaN reciprocal lattice points (RLPs) gets closer to the fully strained position, indicating more pseudomorphic behavior.

AlGaN is well suited for DUV optoelectronics due to its direct ultrawide bandgap and the ability to cover the UV-A, UV-B, and UV-C spectra through precise alloy composition tuning. Figure 4(a) shows the room temperature photoluminescence characteristics of the AlGaN samples. For photoluminescence experiments, the sample was excited with a 193 nm ArF excimer laser, and photoluminescence emission was collected and analyzed by a Horiba iHR550 spectrometer equipped with a UV-sensitive Symphony II CCD detector.

By adjusting the Al/Ga flux ratio, the Al composition in the Npolar AlGaN films was systematically tuned from 0% (GaN) to 20%, 40%, 65%, and 100% (AlN). This controlled variation was verified by the shift in the band edge emission peak position observed in the corresponding photoluminescence spectrum. Despite significant advancements in AlGaN-based materials and devices, the successful integration of AlGaN-based optoelectronic devices, especially those requiring high Al compositions, faces substantial hurdles, primarily attributed to the formidable challenge of attaining high-quality material. AlGaN alloys, when grown heteroepitaxially on sapphire and silicon substrates, commonly encounter a notable presence of both extended and point defects owing to a large lattice mismatch. Employing SiC as the substrate, as reported in this work, is an effective approach to circumvent this challenge owing to a more favorable lattice approximation with Al(Ga)N. Additionally, the formation of three-dimensional (3D) island-like growth modes, particularly in Npolar growth, is influenced by the high adhesion coefficient and low surface migration velocity of Al atoms, leading to an elevated dislocation density in AlGaN epilayers. These dislocations typically serve as nonradiative recombination centers in active devices based on AlGaN.<sup>35</sup> In the present study, a relatively high growth temperature along with a high metal flux helps to enhance the adatom mobility and yet maintain a residual metal flux to compensate for the adsorption at elevated temperatures, resulting in high-quality N-polar AlGaN films.

To assess the radiative recombination efficiency of epitaxially grown AlGaN, temperature-dependent photoluminescence measurements were conducted. Figure 4(b) presents the PL spectra of  $Al_{0.65}Ga_{0.35}N$  as the temperature decreases from 300 to 12 K while

maintaining a pumping power of 30  $\mu$ W. The estimation of internal quantum efficiency (IQE) values was achieved by comparing the integrated intensity of the photoluminescence emission at room temperature (RT) to that at low temperature (12 K), assuming that IQE at 12 K is 100% due to the inactivation of defect-related nonradiative recombination centers.<sup>36</sup> As shown in Fig. 4(c), a high IQE  $\sim$ 74% was observed for the Al<sub>0.65</sub>Ga<sub>0.35</sub>N sample, demonstrating a large radiative recombination rate and suggesting an absence of significant defects or dislocations in the epitaxially grown films. The formation of Ga-rich nanoclusters has been commonly observed in AlGaN epilayers.<sup>37</sup> The resulting charge carrier localization and quantum-confinement contributes to the significantly enhanced photoluminescence intensity and high IQE.38 The formation of Ga-rich nanoclusters in the AlGaN epilayers also leads to significant asymmetric broadening of the PL spectrum to higher wavelengths for AlGaN epilayers compared to GaN or AlN, as observed in Fig. 4(b).

To seamlessly integrate with existing electronic and optoelectronic platforms, successful doping and precise control of conductivity are crucial. While achieving controllable n-doping in low Al content AlGaN films is well documented, it proves to be challenging to attain highly conductive AlGaN with a high Al content. <sup>39</sup> This difficulty primarily arises from factors such as dislocation densities, high donor activation energy, compensation effects caused by acceptor-like defects, negatively charged Al, Ga vacancies, and Si DX centers. <sup>40,41</sup> Therefore, our study focuses on Si doping in high Al content (65%) N-polar AlGaN films. We employed Hall-effect measurements in a standard van der Pauw geometry to thoroughly investigate the electrical properties.

The carrier concentrations measured in Al $_{0.65}$ Ga $_{0.35}$ N epilayers are shown in Fig. 5(a) for five different Si cell temperatures, ranging from 1125 to 1225 °C. Effective modulation of the electron concentration is achieved, spanning several orders of magnitude, which greatly enhances the versatility of Si-doped N-polar AlGaN in various application domains. The relationship between mobility and Si cell temperature is also illustrated in Fig. 5(a). The highest mobility value of  $\sim\!65\,\mathrm{cm^2/V}\text{-}s$  is observed corresponding to an electron concentration of  $1.1\times10^{17}\,\mathrm{cm^{-3}}$ . Notably, even at the higher range of doping, a relatively high mobility value of  $18\,\mathrm{cm^2/V}\text{-}s$  is sustained for an electron concentration of  $3.2\times10^{19}\,\mathrm{cm^{-3}}$ . This finding highlights the feasibility

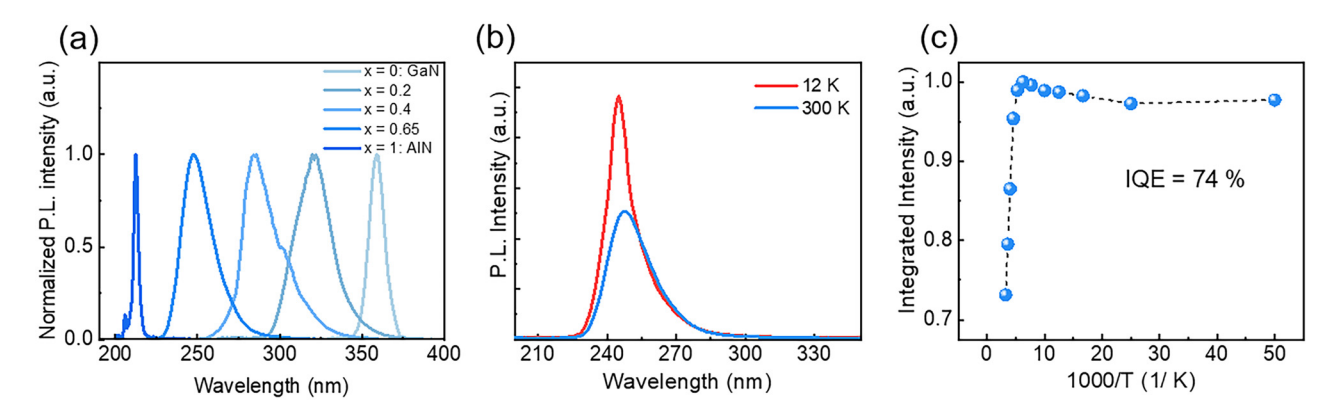


FIG. 4. (a) Normalized photoluminescence (PL) intensity plots showing compositional tunability in N-polar  $Al_xGa_{1-x}N$ , from x=0% (GaN) to 20%, 40%, 65%, and 100% (AlN). (b) Temperature-dependent PL spectra of the 65% Al content AlGaN sample at 12 and 300 K. (c) Variations of the integrated PL intensity vs temperature for a 200 nm  $Al_{0.65}Ga_{0.35}N$  epilayer.

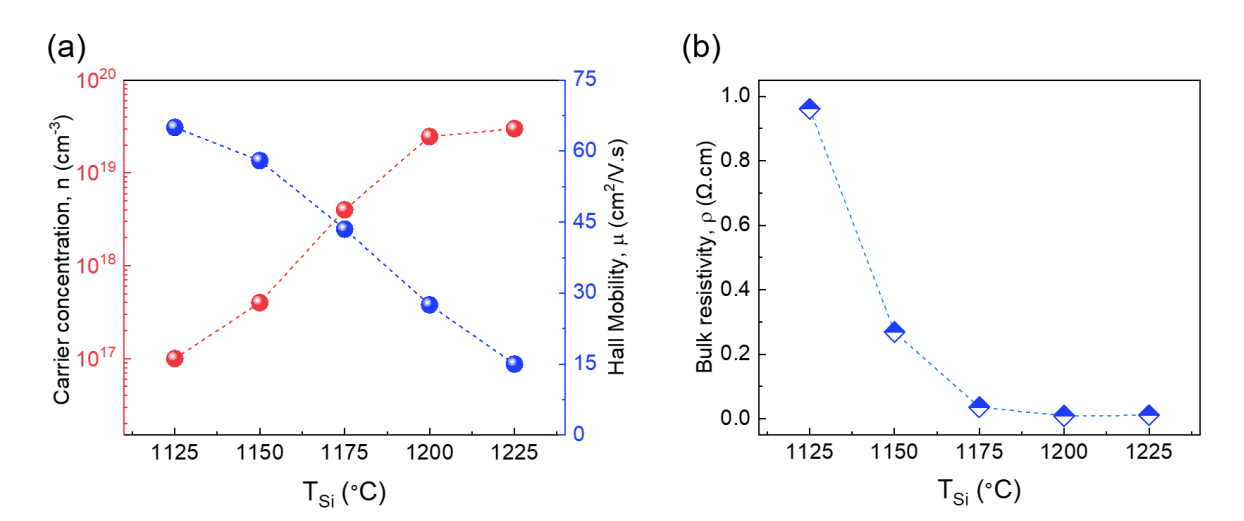


FIG. 5. (a) Plot of carrier concentration and Hall mobility for Si-doped AlGaN epilayers with varying Si cell temperature. (b) Bulk resistivity as a function of silicon cell temperature for the 200 nm 65% Al content AlGaN epilayer.

TABLE I. Benchmarking of resistivity for high AI content AIGaN films.

REFERENCE	COMPOSITION	THICKNESS	$ ho_{ m  BULK}  (\Omega  { m CM})$	GROWTH METHOD
42	Al <sub>0.77</sub> Ga <sub>0.23</sub> N	1.5 μm	0.033	MOCVD
43	$Al_{0.62}Ga_{0.38}N$	$1.3~\mu\mathrm{m}$	0.0066	MOVPE
44	$Al_{0.6}Ga_{0.4}N$	$1.05~\mu\mathrm{m}$	0.04	MOVPE
45	$Al_{0.6}Ga_{0.4}N$	$1\mu\mathrm{m}$	0.05	MOCVD
46	$Al_{0.7}Ga_{0.3}N$	150 nm	0.044	MBE
39	$Al_{0.7}Ga_{0.3}N$	400 nm	0.05	MOVPE
20	$Al_{0.54}Ga_{0.46}N$	600 nm	0.014	MOCVD
This work	$Al_{0.65}Ga_{0.35}N$	200 nm	0.009	MBE

of maintaining desirable mobility characteristics across a wide range of doping levels. The Si-doped AlGaN films demonstrated exceptional electrical conductivity [shown in Fig. 5(b)], as indicated by the lowest resistivity value of  $0.009\,\Omega$ .cm reported for AlGaN in a similar compositional range. Table I presents a comparison with some of the lowest resistivity Si-doped high Al content AlGaN films reported in the literature.

The benchmarking results shown in Table I demonstrate that the Si-doped high Al content N-polar AlGaN epilayers in this study exhibit remarkably low resistivity values within the specified thickness range, which also suggests that the formation of  $V_{\rm Al}+n{\rm Si}_{\rm Al}$  complexes and other self-compensating factors is suppressed.  $^{39,40}$  Moreover, such a low resistivity obtained for the Si-doped AlGaN films suggests a transition to a metallic conductivity state in the higher doping range, as has been demonstrated recently for highly doped  $n\text{-Al}_{0.7}{\rm Ga}_{0.3}{\rm N}$  films  $(>10^{19}\,{\rm cm}^{-3})$  with vanishing effective dopant activation energy, suggesting almost all the Si dopants are effectively activated in this range of doping.  $^{46}$ 

In summary, we demonstrate high-quality N-polar AlGaN films on C-face 4H-SiC substrates with compositions varying across the entire alloy range, which exhibit atomically smooth surface, high luminescence emission efficiency in the deep UV, and excellent charge carrier transport properties. The achievement of N-polar AlGaN directly on SiC wafers, with exceptional structural, electrical, and optical attributes, provides a promising trajectory for future developments of high-power, high-frequency, and high-temperature electronics. Furthermore, this study is instrumental for substantial progress in achieving high efficiency deep UV optoelectronics and photonics.

This work was supported by U.S. Army Research Office under Grant Nos. W911NF2310142 and W911NF-22-2-0176 and National Science Foundation under Grant No. 2026484. Bhuiyan and Zhao would like to acknowledge funding support from the Office of Naval Research (No. N00014-23-1-2640). The authors thank Professor Becky (R.L.) Peterson at the University of Michigan for her generous support and help with the Hall measurements.

### AUTHOR DECLARATIONS Conflict of Interest

Some IP related to this work has been licensed to NS Nanotech, Inc., which was co-founded by Zetian Mi. The University of Michigan and Mi have a financial interest in the company.

### **Author Contributions**

Shubham Mondal: Conceptualization (equal); Data curation (equal); Formal analysis (equal); Investigation (equal); Methodology (equal); Writing – original draft (equal). Ding Wang: Conceptualization (equal); Methodology (equal); Supervision (equal); Validation (equal); Writing – review & editing (equal). A F M Anhar Uddin Bhuiyan: Data curation (equal); Investigation (equal); Writing – review & editing (equal). Mingtao Hu: Data curation (equal); Investigation (equal). Maddaka Reddeppa: Data curation (equal); Investigation (equal). Ping Wang: Conceptualization (equal); Investigation (equal); Methodology (equal); Supervision (equal); Validation (equal). Hongping Zhao: Conceptualization (equal); Funding acquisition (equal); Resources (equal); Supervision (equal); Writing – review & editing (equal). Zetian Mi: Conceptualization (equal); Funding acquisition (equal); Resources (equal); Supervision (equal); Writing – review & editing (equal).

### **DATA AVAILABILITY**

The data that support the findings of this study are available from the corresponding author upon reasonable request.

### REFERENCES

- <sup>1</sup>Y. Wu, X. Liu, A. Pandey, P. Zhou, W. J. Dong, P. Wang, J. Min, P. Deotare, M. Kira, E. Kioupakis, and Z. Mi, Prog. Quantum Electron. 85, 100401 (2022).
- <sup>2</sup>T. Palacios, C.-S. Suh, A. Chakraborty, S. Keller, S. P. DenBaars, and U. K. Mishra, IEEE Electron Device Lett. 27(6), 428 (2006).
- <sup>3</sup>S. Vanka, E. Arca, S. Cheng, K. Sun, G. A. Botton, G. Teeter, and Z. Mi, Nano Lett. **18**(10), 6530 (2018).
- <sup>4</sup>O. Ambacher, J. Phys. D: Appl. Phys. **31**(20), 2653 (1998).
- <sup>5</sup>T. Palacios, F. Calle, J. Grajal, E. Monroy, M. Eickhoff, O. Ambacher, and F. Omnes, Presented at the 2002 IEEE Ultrasonics Symposium, 2002. Proceedings, 2002.
- <sup>6</sup>A. Pandey, J. Gim, R. Hovden, and Z. Mi, Appl. Phys. Lett. 117(24), 241101 (2020).
- <sup>7</sup>H. Hirayama, S. Fujikawa, and N. Kamata, Electron. Commun. Jpn. **98**(5), 1 (2015).
- <sup>8</sup>D. Li, S. Liu, Z. Qian, Q. Liu, K. Zhou, D. Liu, S. Sheng, B. Sheng, F. Liu, and Z. Chen, Adv. Mater. 34(19), 2109765 (2022).
- <sup>9</sup>J.-G. Kim, C. Cho, E. Kim, J. S. Hwang, K.-H. Park, and J.-H. Lee, IEEE Trans. Electron Devices **68**(4), 1513 (2021).
- <sup>10</sup>U. K. Mishra, P. Parikh, and Y.-F. Wu, Proc. IEEE 90(6), 1022 (2002).
- <sup>11</sup>T. Palacios, A. Chakraborty, S. Rajan, C. Poblenz, S. Keller, S. P. DenBaars, J. S. Speck, and U. K. Mishra, <u>IEEE Electron Device Lett.</u> 26(11), 781 (2005).
- <sup>12</sup>A. M. Armstrong, B. A. Klein, A. Colon, A. A. Allerman, E. A. Douglas, A. G. Baca, T. R. Fortune, V. M. Abate, S. Bajaj, and S. Rajan, Jpn. J. Appl. Phys., Part 1 57(7), 074103 (2018).
- <sup>13</sup>S. Keller, H. Li, M. Laurent, Y. Hu, N. Pfaff, J. Lu, D. F. Brown, N. A. Fichtenbaum, J. S. Speck, and S. P. DenBaars, Semicond. Sci. Technol. 29(11), 113001 (2014)
- <sup>14</sup>Z. Zhuang, D. Iida, and K. Ohkawa, Opt. Express 28(21), 30423 (2020).
- <sup>15</sup>O. S. Koksaldi, J. Haller, H. Li, B. Romanczyk, M. Guidry, S. Wienecke, S. Keller, and U. K. Mishra, IEEE Electron Device Lett. 39(7), 1014 (2018).

- <sup>16</sup>S. Dasgupta, Nidhi, N. David, F. Brown, F. Wu, S. Keller, J. S. Speck, and U. K. Mishra, Appl. Phys. Lett. **96**(14), 143504 (2010).
- <sup>17</sup>A. Pandey and Z. Mi, IEEE J. Quantum Electron. 58(4), 1 (2022).
- <sup>18</sup>P. Wang, D. Wang, S. Mondal, Y. Wu, T. Ma, and Z. Mi, ACS Appl. Mater. Interfaces 14(13), 15747 (2022).
- <sup>19</sup>S. Dasgupta, F. Wu, J. S. Speck, and U. K. Mishra, Appl. Phys. Lett. **94**(15), 151906 (2009).
- <sup>20</sup>S. Xu, X. Zhang, X. Luo, R. Fang, J. Lyu, M.-J. Lai, and G. Hu, Mater. Sci. Semicon. Process. **160**, 107447 (2023).
- <sup>21</sup>O. Ledyaev, M. Pandikunta, and S. Nikishin, Jpn. J. Appl. Phys., Part 1 53(5), 050306 (2014).
- <sup>22</sup>J. Singhal, J. Encomendero, Y. Cho, L. van Deurzen, Z. Zhang, K. Nomoto, M. Toita, H. G. Xing, and D. Jena, AIP Adv. 12(9), 095314 (2022).
- <sup>23</sup>Z. Zhang, Y. Hayashi, T. Tohei, A. Sakai, V. Protasenko, J. Singhal, H. Miyake, H. G. Xing, D. Jena, and Y. Cho, Sci. Adv. 8(36), eabo6408 (2022).
- <sup>24</sup>L. Jori, H. Okumura, I. Kim, C. Kauppinen, T. Palacios, and S. Suihkonen, J. Cryst. Growth 487, 12 (2018).
- <sup>25</sup>L. Jori, H. Okumura, I. Kim, M. Rudzinski, J. Grzonka, T. Palacios, and S. Suihkonen, J. Cryst. Growth 487, 50 (2018).
- <sup>26</sup>D. Won and J. M. Redwing, J. Cryst. Growth 377, 51 (2013).
- <sup>27</sup>J. Choi, R. Puthenkovilakam, and J. P. Chang, Appl. Phys. Lett. 86(19), 192101 (2005).
- <sup>28</sup>J. Lu, J.-T. Chen, M. Dahlqvist, R. Kabouche, F. Medjdoub, J. Rosen, O. Kordina, and L. Hultman, Appl. Phys. Lett. 115(22), 221601 (2019).
- <sup>29</sup>A. Yoshikawa and K. Xu, Opt. Mater. **23**(1-2), 7 (2003).
- <sup>30</sup>H. Morkoç, J. Mater. Sci. **12**, 677 (2001).
- <sup>31</sup>X. W. Chen, C. H. Jia, Y. H. Chen, H. T. Wang, and W. F. Zhang, J. Phys. D: Appl. Phys. 47(12), 125303 (2014).
- <sup>32</sup>Q. Sun, Y. S. Cho, I.-H. Lee, J. Han, B. H. Kong, and H. K. Cho, Appl. Phys. Lett. 93(13), 131912 (2008).
- <sup>33</sup>M. Adachi, M. Takasugi, M. Sugiyama, J. Iida, A. Tanaka, and H. Fukuyama, Phys. Status Solidi B 252(4), 743 (2015).
- 34Y. Nagasawa and A. Hirano, Appl. Sci. 8(8), 1264 (2018).
- 35S. F. Chichibu, A. Uedono, K. Kojima, H. Ikeda, K. Fujito, S. Takashima, M. Edo, K. Ueno, and S. Ishibashi, J. Appl. Phys. 123(16), 161413 (2018).
- <sup>36</sup>A. Getty, E. Matioli, M. Iza, C. Weisbuch, and J. S. Speck, Appl. Phys. Lett. 94, 181102 (2009).
- <sup>37</sup>S. Zhao, S. Woo, M. Bugnet, X. Liu, J. Kang, G. Botton, and Z. Mi, Nano Lett. 15(12), 7801–7807 (2015).
- <sup>58</sup>H. Sun, S. Mitra, R. C. Subedi, Y. Zhang, W. Guo, J. Ye, M. K. Shakfa, T. K. Ng, B. S. Ooi, and I. S. Roqan, Adv. Func. Mater. 29(48), 1905445 (2019).
- <sup>39</sup>R. Collazo, S. Mita, J. Xie, A. Rice, J. Tweedie, R. Dalmau, and Z. Sitar, Phys. Status Solidi C 8(7-8), 2031 (2011).
- <sup>40</sup> A. Kakanakova-Georgieva, D. Nilsson, X. T. Trinh, U. Forsberg, N. T Son, and E. Janzén, Appl. Phys. Lett. **102**(13), 132113 (2013).
- <sup>41</sup>K. B. Nam, J. Li, M. L. Nakarmi, J. Y. Lin, and H. X. Jiang, Appl. Phys. Lett. 81(6), 1038 (2002).
- <sup>42</sup>J. Y. Lin and H. X. Jiang, J. Appl. Phys. **113**(12), 123501 (2013).
- <sup>43</sup>K. Nagata, H. Makino, T. Yamamoto, K. Kataoka, T. Narita, and Y. Saito, Appl. Phys. Express 13(2), 025504 (2020).
- <sup>44</sup>P. Pampili, D. V. Dinh, V. Z. Zubialevich, and P. J. Parbrook, J. Phys. D: Appl. Phys. 51(6), 06LT01 (2018).
- <sup>45</sup>M. Pophristic, S. P. Guo, and B. Peres, Appl. Phys. Lett. **82**(24), 4289 (2003).
- <sup>46</sup>S. Bharadwaj, S. M. Islam, K. Nomoto, V. Protasenko, A. Chaney, H. G. Xing, and D. Jena, Appl. Phys. Lett. **114**(11), 113501 (2019).